ACS Photonics

Letter

pubs.acs.org/journal/apchd5

Large-Area, Lithography-Free Super Absorbers and Color Filters at Visible Frequencies Using Ultrathin Metallic Films

Zhongyang Li,[†] Serkan Butun,[†] and Koray Aydin*

Department of Electrical Engineering and Computer Science, Northwestern University, Evanston, Illinois 60208, United States

Supporting Information

ABSTRACT: Nanostructured photonic materials enable control and manipulation of light at subwavelength scales and exhibit unique optical functionalities. In particular, plasmonic materials and metamaterials have been widely utilized to achieve spectral transmission, reflection, and absorption filters based on localized or delocalized resonances arising from the interaction of photons with nanostructured materials. Realization of visible-frequency, high-performance, large-area, optical filters based on nanoplasmonic materials is rather challenging due to nanofabrication related problems (cost, fabrication imperfection, surface roughness) and optical losses of metals. Here, we propose and demonstrate large-area perfect absorbers and transmission filters that overcome difficulties associated with the nanofabrication using a lithography-free approach. We also utilize and benefit from the optical losses in metals in our optical filter designs. Our resonant optical filter design is based on a modified, asymmetric metal−insulator−metal (MIM) based Fabry−Perot cavity with plasmonic, lossy ultrathin (~30 nm) metallic films used as the top metallic layer. We demonstrated a narrow bandwidth (~17 nm) super absorber with 97% maximum absorption with a performance comparable to nanostructure/nanoparticle-based super absorbers. We also investigated transmission (color) filters using ultrathin metallic films, in which different colors can be obtained by controlling the dielectric spacer thickness. With performance parameters of transmittance peak intensity reaching 60% and a narrow-band of ~40 nm, our color filters exceed the performance of widely studied plasmonic nanohole array based color filters. Proposed asymmetric Fabry−Perot cavities using ultrathin metallic films could find applications in spectrally selective optical (color and absorber) filters, optoelectronic devices with controlled bandwidth such as narrow-band photodetectors, and light-emitting devices.

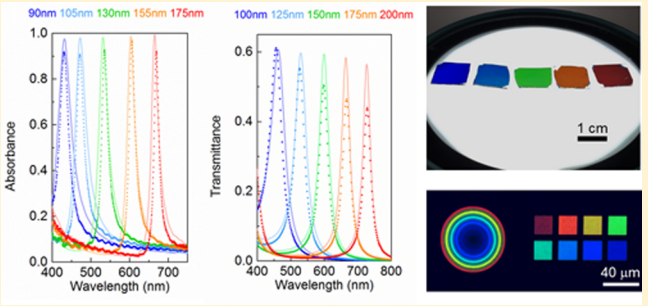

KEYWORDS: *super absorbers, color filters, lithography-free, ultrathin films, metal−insulator−metal, flat optics*

Plasmonic nanostructures and metamaterials provide an unprecedented amount of opportunities in controlling and manipulating light−matter interactions at the nanoscale and enable spectral engineering of many optical processes including transmission, reflection, absorption, and emission of light. In general, unique optical properties in such artificial engineered nanophotonic materials emerge from optical resonances induced by nanostructures, therefore, spectral information depend strongly on the size, shape, and periodicity of metallic and dielectric nanostructures. In recent years, plasmonic materials and metamaterials have received a burgeoning amount of interest from the scientific community due to their exciting optical functions such as field localization, refractive index engineering, phase and amplitude control, and many more. Controlling the spectral transmission, reflection, and absorption properties of materials is of special interest, in particular, perfect absorbers and transmission (color) filters based on metallic nanostructures has been widely studied. It has been shown that almost perfect absorbers with zero reflectance and transmittance can be realized by designing metamaterials with an effective impedance matched to that of free space[1] or fabricating metallic nanostructures on a dielectric/metallic substrate.[1−6] Since perfect absorbers based on plasmonic nanostructures and optical metamaterials operating at visible frequencies require subwavelength features, large-area, and high-precision nanofabrication techniques are required for functional visible-frequency perfect absorbers.

On the other hand, planar, multilayer thin-film coatings can be designed as Bragg-reflector or Fabry−Perot cavities to yield resonant enhancement in various optoelectronic devices such as light emitting diodes (LED), photodetectors,[7−9] photovoltaics,[10,11] surface photocatalysis, phototransistors,[12] modulators,[13] and amplifier.[13] Such planar optical devices can be traced back to a bulky, triple-layer structure known as Salisbury Screen (SS), which is designed for radar wave absorption.[14] More recently, several studies demonstrated strong resonant/absorptive characteristics from double-layer thin-film coatings[15,16] or metal−insulator−metal triple-layer[17,18] or multilayer[19,20] coatings in microwave, infrared (IR) spectrum and beyond. Particularly, in a recent work,[15] Kats et al. investigated strong optical interference effects in ultrathin, absorptive

Received: October 31, 2014
Published: January 28, 2015

DOI: 10.1021/ph500410u
ACS Photonics 2015, 2, 183−188

Germanium films coated on metallic mirrors and demonstrated that continuous, absorptive thin films with subwavelength thicknesses can indeed engineer the optical reflection and absorption spectra. This recent study renewed the interest in continuous, thin film based optical devices and proved that ultrathin continuous films are worth exploring as alternative candidates for spectral engineering of optical properties that are controlled solely by the film thickness rather than in-plane, nano/microstructure size. Continuous, unstructured thin films involve only smooth planar surfaces, enabling high-throughput, large-area, lithography-free fabrication only by depositing thin films on required substrates, therefore, not requiring costly nanofabrication techniques

Here, we report large-area, lithography-free near-perfect (super) absorbers and transmission color filters based on triple-layer, metal−insulator−metal (MIM) thin-film stacks operating at visible frequencies. Super absorbers based on nanoparticles/nanostructures have previously shown to have broadband[3,4] or narrow-band[2,5,21−23] spectral characteristics. Resonant super absorbers are promising for various applications, including photovoltaics, photodetectors, photothermal therapy,[24] thermophotovoltaics,[3] heat-assisted magnetic recording,[25] hot-electron collection,[26] biochemical sensing,[2] and thermal emitting.[1−6,15,16]

RESULTS AND DISCUSSION

Lossless dielectric materials with high index contrast have been widely used to support strong interference effects, which depends on multiple pass light circulation in order to achieve antireflection/high-reflection coatings,[27,28] as well as optical filters.[29] For the energy harvesting/conversion purposes, materials with high dissipation (metals or semiconductors) need to be incorporated in the resonant cavity designs. However, lossy materials such as metals, reduce the quality factor of optical cavities by inducing attenuation and perturbation for propagation/trapped waves.[20,30] Partially reflecting mirrors have been used as resonant Fabry−Perot cavities for designing lasers, in which optical losses from lossy mirrors can be compensated by the gain media. Here, we present planar thin-film coatings comprised of MIM cavities, that is, a thin metallic layer coupled through a dielectric spacer with the bottom metallic thick layer. The representative geometry is schematically shown in Figure 1a with size parameters of top Ag thickness t, middle SiO_2 thickness d, and bottom Ag thickness h. In this study, we will present two potential applications of such thin metallic multilayer films, namely, super absorbers and color filters.

Super Absorbers. For the design of super absorbers, we intentionally chose the bottom metal layer thickness to be optically thick (h = 100 nm) in order to minimize light transmission. To optimize the trade-off between light penetration into the planar nanocavity and material losses, top metallic film thickness t is set to be 30 nm. This thickness allows for the balance between strong cavity confinement and light coupling (details are described in the following context and also Supporting Information).

The simulated reflectance spectra are obtained by performing full wave Finite-Difference Time-Domain (FDTD) method for the planar MIM cavity. The complex refractive index of Ag and SiO_2 is used from data of Palik.[31] A plane wave is normally incident to the top surface of MIM cavity. Figure 1b shows a plot of the reflectance spectra as a function of SiO_2 thickness and the wavelength. As shown in Figure 1b, the reflectance dip

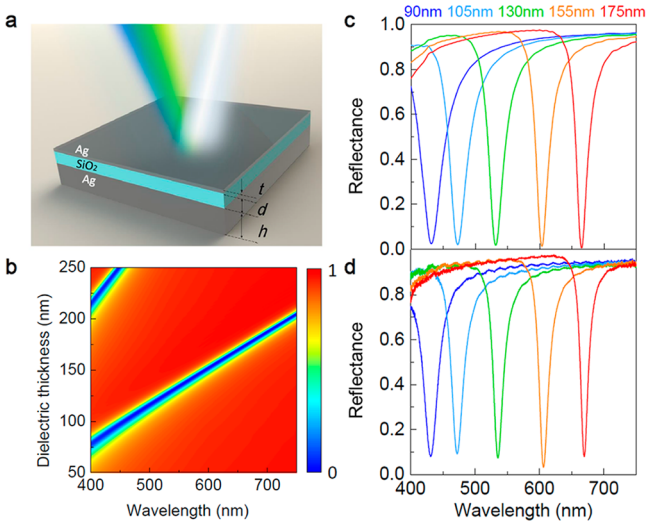

Figure 1. Schematic configurations and reflectivity spectra of planar thin-film MIM cavity. (a) Schematic drawing of planar Ag/SiO_2/Ag cavity. The thickness of top and bottom metallic layers are set to be t = 30 nm and h = 100 m. The illumination source is normally incident onto the planar surface with arbitrary polarization. (b) Reflectance plotted as a function of wavelength and dielectric thickness d. (c) Simulated and (d) measured reflectance spectra for MIM cavity with SiO_2 spacer thicknesses of d = 90, 105, 130, 155, and 175 nm.

is shifting from ∼400 nm continuously to ∼750 nm as a function of the dielectric thickness d from ∼75 to ∼200 nm, covering the entire visible frequency domain. A higher order mode starts to appear around 400 nm, when dielectric thickness d is over 200 nm. In order to experimentally validate this effect, we deposited various multilayer Ag/SiO_2/Ag cavities with five different oxide thicknesses on a polished silicon wafer using electron-beam (E-beam) evaporation. The oxide thickness variations (d = 90, 105, 130, 155, and 175 nm) are realized by etching the same oxide thickness coatings for different processing duration in reactive-ion etching (RIE) facility. Reflectance measurements are performed using an inverted optical microscope setup. The simulated and measured reflectance spectra for five different MIM cavities with varying oxide thicknesses are plotted in Figure 1c,d. Our experimental and numerical results indicate that continuous three-layer MIM cavities enable strong optical interference effects and reduce reflection significantly from an otherwise conductive, highly reflective surface. The full width at half-maximum (fwhm) for the measured resonances is ∼14−28 nm, giving rise to quality factor (Q-factor) as high as ∼48 ($Q = (\lambda/\Delta\lambda)$).

Since the bottom metallic layer is optically thick, incident light is not transmitted through these films. Therefore, one can calculate the absorbance (A) of thin-film coating is using a simple formula $A = 1 - R - T$ (T = 0), where R and T represent the reflectance and transmittance, respectively. We plotted simulated (solid lines) and measured (dots) absorption spectra of five MIM films in Figure 2a. The overall shape and position of experimental spectral features match quite well with the simulated ones. The maximum absorption reaches over 99.5% in simulation and close to 96.8% in experiment. Specific performance parameters are listed in Table S1 in the Supporting Information.

In order to visualize and better understand the absorption mechanism in three-layer MIM cavity, we calculated the total electric field (E-field) intensity (Figure 2b) and the absorbed

DOI: 10.1021/ph500410u
ACS Photonics 2015, 2, 183−188

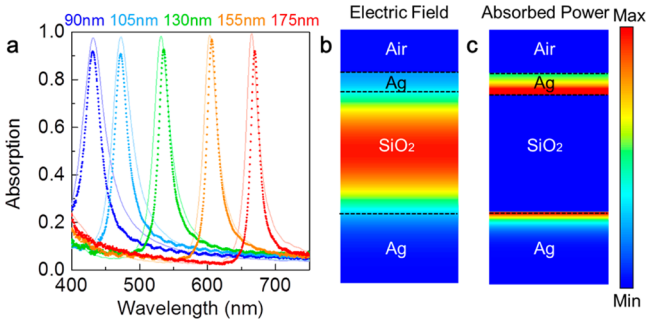

Figure 2. Near-perfect absorption by asymmetric Fabry–Perot-type cavity. (a) Measured (dots) and simulated (solid lines) absorptivity spectra for MIM cavity with different dielectric (SiO_2) thickness d = 90, 105, 130, 155, and 175 nm. (b) Electric field intensity profile and (c) absorbed power distribution for the MIM filter (d = 155 nm) at the maximum absorption peak wavelength of 607 nm.

power (Figure 2c) at the absorption resonance peak for the cavity with 155 nm thick oxide. The *E*-field is highly confined at the dielectric section between two metallic films, where a standing wave is formed due to constructive interference of incoming and reflected waves. Due to the enhanced electric field resulting from the cavity effect, most of the optical power is absorbed inside the top metallic film (Figure 2c). Absorption map reveals that absorption is higher at the metal–dielectric interfaces (both at the top as well as at the bottom interface). It is rather interesting to achieve almost perfect absorption using continuous metallic films. The planar MIM cavity is not relying any plasmonic effect, but essentially an asymmetric Fabry–Perot-type (FP-type) resonator, comprised of lossless core dielectric with partially reflective top metal layer and optically thick, highly reflective mirror. The resonance condition is associated with the multiple round-trip phase shifts of electromagnetic wave inside the resonant cavity.[18] Nevertheless, owing to the dispersive nature of incorporated metal and its inherent resistive perturbation in films that is much thinner than the wavelength, the interface reflection and transmission phase changes along with the wave attenuation become nontrivial and render the resonant nanocavity studied here distinctive from conventional FP perspective.[20,30,32−34] A conventional lossless FP dielectric cavity usually induced strong destructive interference by effective optical path of quarter wavelength to modulate transmission and reflection spectra but without any absorption involved. Here, the top metallic thickness plays a critical role in achieving almost perfect absorption, which will be discussed later in detail.

In general, super absorbers operating at optical frequencies utilize nano and microstructured surfaces that require nanolithography and other processing techniques such as lift-off for patterning. In comparison with these nanostructure/nanoparticle-based absorbers,[2−5,22] the absorption bands in our proposed MIM planar cavities are quite sharp (~8–15 nm) with high, comparable peak absorption amplitude (~97%). Moreover, the absorption mechanisms in absorbers that utilize nanostructured materials usually depend on localized surface plasmon resonances (LSPR), which is highly susceptible to the inhomogeneity of features and surface roughness caused during the fabrication processes. MIM-based absorbers proposed in this study involve subwavelength thickness films of metals and dielectrics that can be deposited using a single electron-beam or thermal deposition tool.

Transmission Color Filters. As an alternative application of MIM films, we investigated transmission (color) filters at visible frequencies by reducing the thickness of bottom Ag film in order to allow light propagation. We explored five different MIM films with varying thicknesses d. Thicknesses of the top and bottom metallic films are chosen to 30 nm for optimum transmission filter performance, after initial electromagnetic simulations. $Ag/SiO_2/Ag$ films are coated on double-side polished, transparent sapphire substrate. Figure 3a shows actual

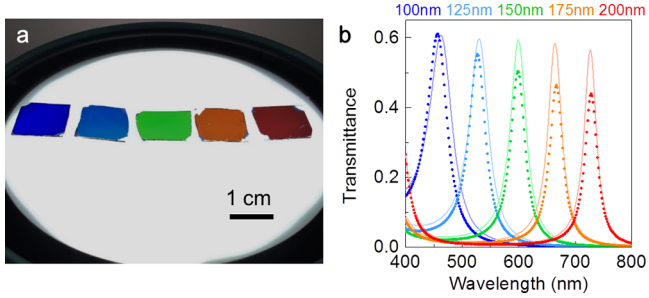

Figure 3. Color filters. (a) Photograph of five different large-area color filters including blue, cyan, green, orange, and wine. MIM samples deposited on double-side polished sapphire substrate with different oxide thickness d. (b) Measured (dots) and simulated (solid lines) transmittance spectra for MIM cavities with different dielectric thickness d = 100, 125, 150, 175, and 200 nm.

fabricated large-area color filters with five different oxide thicknesses. A white light source is excited from the back side of the filters and one can see vivid, bright colors of blue, cyan, green, orange and wine. Since the actual mechanism resulting in spectral selectivity in the transmission mode is due to the constructive interference, the angle of incidence would affect the color. Angle-dependent characteristics of color filter are observed as shown in Figures S2 and S3 of Supporting Information and more discussion on spectral shifting feature can be found correspondingly.

Measured and simulated transmittance spectra for five MIM cavities with different oxide thicknesses are plotted in Figure 3b. An increase in thickness of dielectric layer d, results in red-shift of the cavity resonance wavelength. For the cases of MIM cavity with oxide thickness $d \sim$ 100, ~125, ~150, ~175, and 200 nm, it is experimentally observed that five transmitted resonance peaks are equally distributed across the entire visible regime (Figure 3b). The maximum transmittance peak obtained in measurement is ~61.6% and the narrowest bandwidth achieved is 29 nm. Excellent agreement is obtained between the measured transmittance spectra (dots) and the simulations (solid lines).

To prove the practical use of MIM transmission filters, we have patterned planar continuous MIM by etching the dielectric spacer layer using focused ion beam (FIB) milling. As shown in Figure 4, the transmission-mode micrographs of different pattern images are fabricated on double-side polished sapphire substrate by combining deposition of thin films and FIB approach.[15,35] As an example, a defined concentric circle pattern (Figure 4a) was created with rainbow colors, in which the thickness of the dielectric layer is altered in a stepwise manner. Furthermore, a color palette consisting of 20 μm × 20 μm squares (Figure 4b) with different dielectric thickness d was fabricated. Potentially, one could fabricate ultrahigh resolution microimage on the resonant cavity by feeding an original image file to the FIB column control software. The software would

DOI: 10.1021/ph500410u
ACS Photonics 2015, 2, 183−188

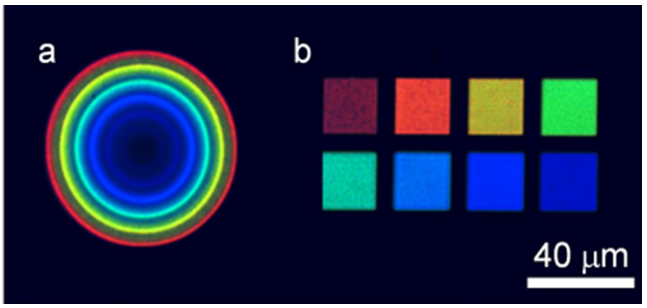

Figure 4. Photographs of colorful images fabricated using focused ion beam (FIB) technique for patterning on the thin films with oxide thickness variation. Among the demonstrated patterns are (a) the rainbow circles and (b) color palettes.

calculate the etch depth as a function of the luminosity data in each pixel of the original image. Depending on the beam size of FIB, the resolution of such microimage could reach over 500 thousand dpi, which is roughly 1000× denser than any average smart phone display. Distinct from the common reflective imaging mode for human eyes, this technology by utilizing nanometer-thick films suggest the potential for transmission-mode design, labeling and visual arts of the future.[15,36]

For both absorption and transmission filters, top metallic silver film layer is chosen to be 30 nm. Note that this is a subwavelength thick metallic film for the operation wavelength range (400−800 nm). At visible frequencies metals do not behave like perfect conductors, therefore there is significant amount of light propagation inside the metal, rendering that metal film thickness is significantly important for the filter performance. This is quite different from conventional Fabry−Perot cavities, in which the thickness of partially reflective mirror is not taken into account. Due to the fact that the metal film used in the MIM filter design has plasmonic behavior at this wavelength, the effective cavity length is modified with the thickness of the metal films.

In order to investigate the effect of metal thickness on the optical performance of absorption and transmission filters, we performed additional numerical simulations and optical measurements. Figure 5a plots the absorption spectra of an MIM absorption filter with dielectric thickness, d = 160 nm and bottom Ag thickness h is ∼100 nm as a function of the top metal film thickness. Figure 5b,c shows the measured and simulated absorption spectra for top metal thicknesses, t = 15, 30, and 45 nm. When increasing the thickness of top metal t between 15 and 45 nm, the bandwidth (fwhm) of absorbance is sharpened remarkably from ∼51 to ∼8 nm. Correspondingly, the thicker metallic boundary serves to boost the Q-factor of nanocavity from ∼10 to ∼75 and contributing to enhanced confinement of trapped wave and stronger wavelength-selective capability. More interestingly, as top metal thickness t increases, the spectral position is not red-shifted, instead blue-shifted slightly from 645 to 623 nm. To clarify the counterintuitive blue-shift, more in-depth discussion of analytical modeling to address the function of top metal layer can be found in Figure S4 of Supporting Information.

In addition to bandwidth control and resonance position modification, there also exhibits an optimum absorptivity when the top Ag thickness t is around 30 nm. To achieve maximum absorption performance, there exists a trade-off between light penetration/coupling into cavity and the metallic losses by amount of the metal used in the filter design. Specifically, a thicker reflective metallic film result in higher reflection from the metal-air interface and will allow less light propagation through the dielectric layer. On the other hand, a thinner metallic film will result in higher transmission and leakage from the MIM cavity after reflecting from the bottom metallic mirror. For the case of t = ∼30 nm, the maximum absorption

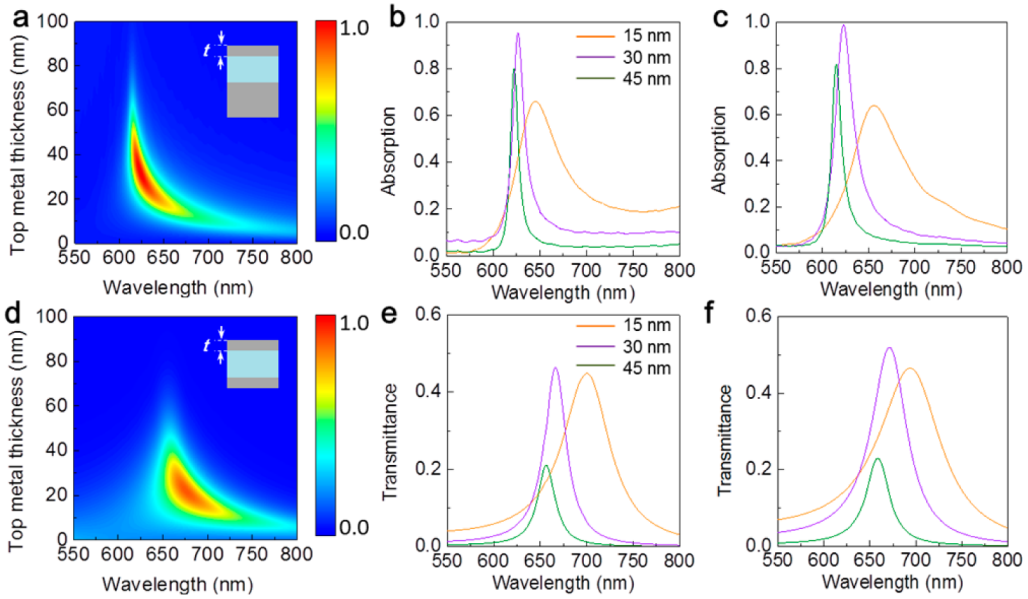

Figure 5. Tunability of resonance peak and bandwidth in absorption and transmittance spectra by top metallic film thickness. (a) Absorption evolution as a function of wavelength and top Ag thickness t in MIM super absorber (d = 160 nm and h = 100 nm). (b) Corresponding measured and (c) simulated absorptivity spectra for MIM absorbers with different top Ag thickness t = 15, 30, and 45 nm. (d) Transmittance evolution as a function of wavelength and top Ag thickness t in MIM transmission filter (d = 175 nm and h = 30 nm). (e) Corresponding measured and (f) simulated transmittance spectra for MIM transmission filters with different top Ag thickness t = 15, 30, and 45 nm.

DOI: 10.1021/ph500410u
ACS Photonics 2015, 2, 183−188

achieved is attributed to optimization the interplay between cavity confinement and thin-film lossy nature.

Similar spectral evolutions are observed for MIM transmission filters upon changing the top boundary Ag layers while keeping the thickness of the middle SiO_2 layer at d = 175 nm and the bottom Ag layer at h = 30 nm, as displayed in Figure 5d−f. Analogous spectral variations to perfect absorbers were exhibited as a function of top Ag layer thickness. In comparison with the reflection-mode cavity with optically thick metal, the spectra for leaking-mode cavity exhibits slightly broader bandwidth due to the weaker confinement from thinner reflective metallic films. To gain more insight into the impact of metal's optical property on absorption performance, we have also studied different metals such as Au/Ag and their hybrid combination for cavity and more discussion can be found in Figure S5 of Supporting Information. As for the stability of the Ag film and its optical performance, these samples of super absorbers and transmission color filters have been measured a couple of times during three months. The Ag surface was observed to be gradually degraded due to oxidation and the resonance intensity was reduced slightly but the spectrum remained the similar line shape.

In conclusion, we have systematically investigated optical properties of asymmetric, modified Fabry−Perot-type cavity using large-area, lithography-free planar MIM coatings, which can be widely applied and integrated to optoelectronic devices including perfect absorbers and color filters at visible and near-IR wavelength range. We proposed and demonstrated a super absorber with a maximum absorption intensity of ∼97% and a fwhm of 8 nm, whose performance is comparable with nanostructured plasmonic material based super absorbers. The thickness and the type of the metal film used in MIM cavity design significantly impacts the bandwidth, absorption, and transmission intensity, the resonance wavelength, and the quality factor of the FP cavities. By optimizing the interplay between the lossy nature of metal and the subwavelength thickness of the metallic films, the FP-type cavity enables high optical confinement of electric field in the middle dielectric layer and enhances optical absorption. By constructing leaking-mode nanocavity, transmission color filters are achieved with over 60% transmittance across the entire visible range and beyond. The high transmission efficiency and ability to realize of wide range of colors by the planar smooth surfaces is quite promising for potential filter and display devices integrated in future commercialized color-CCD/camera. Distinctive from the conventional reflective images for human eyes, this technology shows promise for transmission-mode design, coloring/labeling, and visual arts of the future. The lithography-free approach based on ultrathin metallic films or potentially 2D atomic materials[9,12,37,38] provides great flexibility and high-throughput manufacturing convenience and open route for low-cost and robust optoelectronic devices based on ultrathin film optical filters.

METHODS

For perfect absorber samples, the bottom Ag layers of ∼100 nm thickness were coated on polished silicon wafer using electron beam (E-beam) evaporator. For transmission filter samples, the thin (30 nm thickness) bottom Ag layers were coated on a double side polished sapphire substrate. Same thickness (∼200 nm) of the SiO_2 layer was deposited onto the bottom Ag layer by E-beam evaporator. The different oxide thicknesses are processed by Reactive Ion Etching (RIE) facility to etch the same SiO_2 thickness coatings for different duration of time. The actual etching rate is ∼33 nm/min. Then 15−45 nm thick top Ag layers were deposited on the surface of SiO_2/Ag coatings by electron-beam evaporator. The micrographs shown in Figure 4 are fabricated through (1) depositing the bottom Ag and SiO_2 layers and (2) etching the patterns on the coating surface using Focus ion beam (FIB) milling and then (3) depositing the top Ag film. By feeding the original image files to the FIB column control software, it could calculate the etching depth as a function of the luminosity data in each pixel of the images.

A microscope equipped with a spectrometer consisting of a 303 mm focal-length monochromator and electron multiplication charge-coupled device (Newton EM-CCD) camera (Andor Technology Ltd.) was utilized for optical characterization. Broad band illumination is generated by a broadband halogen lamp and a linear polarizer was inserted into the light pathway to polarize the incident light. Reflected and transmitted light was collected using a 2× Nikon microscope objective with a numerical aperture of 0.06. For calibration of reflection, we first measured the reflectance from a broadband dielectric mirror (Edmund Optics #64−114) with an average reflectance of 99% between 350 and 1100 nm. Measured reflectance from MIM samples was then calibrated using the reflectance spectra of the dielectric mirror.

Full-field electromagnetic wave calculations were performed using Lumerical, a commercially available finite-difference time-domain (FDTD) simulation software package. Simulations for the planar MIM films were performed in 2D layout. A unit cell of 200 nm along the x-axis was selected for the planar structure and was simulated using periodic boundary conditions along the x-axis and perfectly matched layers (PML) along the propagation of electromagnetic waves (y-axis). Plane waves were launched incident to the unit cell along the $+y$ direction, and reflection is collected with a power monitor placed behind the radiation source; transmission is collected with a power monitor placed behind the structure. Electric and magnetic field distribution cross-section are detected by a 2D field profile monitors in x−y plane. The complex refractive index of Ag for simulation is utilized from the data of Palik (0−2 μm)[31] and SiO_2 is from the data of Palik.[31]

ASSOCIATED CONTENT

Supporting Information

More details of angle-dependent characteristics and analytical modeling for thickness variation of top metal layer. This material is available free of charge via the Internet at http://pubs.acs.org.

AUTHOR INFORMATION

Corresponding Author

*E-mail: aydin@northwestern.edu.

Author Contributions

†These authors equally contributed to this work (Z.L. and S.B.).

Notes

The authors declare no competing financial interest.

ACKNOWLEDGMENTS

This material is based on work supported by the AFOSR under Award No. FA9550-12-1-0280. K.A. acknowledges financial support from the McCormick School of Engineering and Applied Sciences at Northwestern University and partial

DOI: 10.1021/ph500410u
ACS Photonics 2015, 2, 183−188

support from the Institute for Sustainability and Energy at Northwestern (ISEN) through ISEN Equipment and Booster Awards. This research was also partially supported by the Materials Research Science and Engineering Center (NSF-MRSEC; DMR-1121262) of Northwestern University. This research made use of the NUANCE Center at Northwestern University, which is supported by NSF-NSEC, NSF-MRSEC, Keck Foundation, the State of Illinois, and the NUFAB cleanroom facility at Northwestern University. Z.L. gratefully acknowledges support from the Ryan Fellowship and the Northwestern University International Institute for Nanotechnology.

REFERENCES

(1) Landy, N.; Sajuyigbe, S.; Mock, J.; Smith, D.; Padilla, W. Perfect metamaterial absorber. *Phys. Rev. Lett.* **2008**, *100*, 207402.
(2) Liu, N.; Mesch, M.; Weiss, T.; Hentschel, M.; Giessen, H. Infrared perfect absorber and its application as plasmonic sensor. *Nano Lett.* **2010**, *10*, 2342−2348.
(3) Aydin, K.; Ferry, V. E.; Briggs, R. M.; Atwater, H. A. Broadband polarization-independent resonant light absorption using ultrathin plasmonic super absorbers. *Nat. Commun.* **2011**, *2*, 517.
(4) Beermann, J.; Eriksen, R. L.; Holmgaard, T.; Pedersen, K.; Bozhevolnyi, S. I. Plasmonic black metals via radiation absorption by two-dimensional arrays of ultra-sharp convex grooves. *Sci. Rep.* **2014**, *4*, 6904.
(5) Hao, J.; Wang, J.; Liu, X.; Padilla, W. J.; Zhou, L.; Qiu, M. High performance optical absorber based on a plasmonic metamaterial. *Appl. Phys. Lett.* **2010**, *96*, 251104−251104−3.
(6) Pala, R. A.; White, J.; Barnard, E.; Liu, J.; Brongersma, M. L. Design of plasmonic thin-film solar cells with broadband absorption enhancements. *Adv. Mater.* **2009**, *21*, 3504−3509.
(7) Kishino, K.; Unlu, M. S.; Chyi, J.-I.; Reed, J.; Arsenault, L.; Morkoc, H. Resonant cavity-enhanced (RCE) photodetectors. *IEEE J. Quantum Electron.* **1991**, *27*, 2025−2034.
(8) Ünlü, M. S.; Strite, S. Resonant cavity enhanced photonic devices. *J. Appl. Phys.* **1995**, *78*, 607−639.
(9) Lopez-Sanchez, O.; Lembke, D.; Kayci, M.; Radenovic, A.; Kis, A. Ultrasensitive photodetectors based on monolayer MoS_2. *Nat. Nanotechnol.* **2013**, *8*, 497−501.
(10) Kim, J. Y.; Kim, S. H.; Lee, H. H.; Lee, K.; Ma, W.; Gong, X.; Heeger, A. J. New architecture for high-efficiency polymer photovoltaic cells using solution-based titanium oxide as an optical spacer. *Adv. Mater.* **2006**, *18*, 572−576.
(11) Dennler, G.; Scharber, M. C.; Brabec, C. J. Polymer-fullerene bulk-heterojunction solar cells. *Adv. Mater.* **2009**, *21*, 1323−1338.
(12) Engel, M.; Steiner, M.; Lombardo, A.; Ferrari, A. C.; Löhneysen, H. v.; Avouris, P.; Krupke, R. Light−matter interaction in a microcavity-controlled graphene transistor. *Nat. Commun.* **2012**, *3*, 906.
(13) Yan, R.; Simes, R.; Coldren, L. Electroabsorptive Fabry-Perot reflection modulators with asymmetric mirrors. *IEEE Photonics Technol. Lett.* **1989**, *1*, 273−275.
(14) Salisbury, W. W. W. Absorbent body for electromagnetic waves. Patent US 2599944 A, 1952.
(15) Kats, M. A.; Blanchard, R.; Genevet, P.; Capasso, F. Nanometre optical coatings based on strong interference effects in highly absorbing media. *Nat. Mater.* **2013**, *12*, 20−24.
(16) Streyer, W.; Law, S.; Rooney, G.; Jacobs, T.; Wasserman, D. Strong absorption and selective emission from engineered metals with dielectric coatings. *Opt. Express* **2013**, *21*, 9113−9122.
(17) Shin, H.; Yanik, M. F.; Fan, S.; Zia, R.; Brongersma, M. L. Omnidirectional resonance in a metal−dielectric−metal geometry. *Appl. Phys. Lett.* **2004**, *84*, 4421−4423.
(18) Yan, M. Metal−insulator−metal light absorber: a continuous structure. *J. Opt.* **2013**, *15*, 025006.
(19) Shu, S.; Yang, L. Y. Metallic rugate structures for near-perfect absorbers in visible and near-infrared regions. *Opt. Lett.* **2012**, *37*, 3495−3497.
(20) Song, H.; Guo, L.; Liu, Z.; Liu, K.; Zeng, X.; Ji, D.; Zhang, N.; Hu, H.; Jiang, S.; Gan, Q. Nanocavity enhancement for ultra-thin film optical absorber. *Adv. Mater.* **2014**, *26*, 2737−2743.
(21) Jiang, Z. H.; Yun, S.; Toor, F.; Werner, D. H.; Mayer, T. S. Conformal dual-band near-perfectly absorbing mid-infrared metamaterial coating. *ACS Nano* **2011**, *5*, 4641−4647.
(22) Moreau, A.; Ciracì, C.; Mock, J. J.; Hill, R. T.; Wang, Q.; Wiley, B. J.; Chilkoti, A.; Smith, D. R. Controlled-reflectance surfaces with film-coupled colloidal nanoantennas. *Nature* **2012**, *492*, 86−89.
(23) Li, Z.; Butun, S.; Aydin, K. Ultranarrow band absorbers based on surface lattice resonances in nanostructured metal surfaces. *ACS Nano* **2014**, *8*, 8242−8248.
(24) Hirsch, L. R.; Stafford, R.; Bankson, J.; Sershen, S.; Rivera, B.; Price, R.; Hazle, J.; Halas, N.; West, J. Nanoshell-mediated near-infrared thermal therapy of tumors under magnetic resonance guidance. *Proc. Natl. Acad. Sci. U.S.A.* **2003**, *100*, 13549−13554.
(25) Stipe, B. C.; Strand, T. C.; Poon, C. C.; Balamane, H.; Boone, T. D.; Katine, J. A.; Li, J.-L.; Rawat, V.; Nemoto, H.; Hirotsune, A. Magnetic recording at 1.5 Pb m^{-2} using an integrated plasmonic antenna. *Nat. Photonics* **2010**, *4*, 484−488.
(26) Knight, M. W.; Sobhani, H.; Nordlander, P.; Halas, N. J. Photodetection with active optical antennas. *Science* **2011**, *332*, 702−704.
(27) Nair, P.; Nair, M.; Garcıa, V.; Arenas, O.; Peña, A. C.; Ayala, I.; Gomezdaza, O.; Sanchez, A.; Campos, J.; Hu, H. Semiconductor thin films by chemical bath deposition for solar energy related applications. *Sol. Energy Mater. Sol. Cells* **1998**, *52*, 313−344.
(28) Lien, S.-Y.; Wuu, D.-S.; Yeh, W.-C.; Liu, J.-C. Tri-layer antireflection coatings (SiO_2SiO_2−TiO_2TiO_2) for silicon solar cells using a sol−gel technique. *Sol. Energy Mater. Sol. Cells* **2006**, *90*, 2710−2719.
(29) Dobrowolski, J. Optical interference filters for the adjustment of spectral response and spectral power distribution. *Appl. Opt.* **1970**, *9*, 1396−1402.
(30) Kats, M. A.; Blanchard, R.; Ramanathan, S.; Capasso, F. Thin-film interference in lossy, ultra-thin layers. *Opt. Photonics News* **2014**, *25*, 40−47.
(31) Palik, E. D. *Handbook of Optical Constants of Solids: Index*; Elsevier: New York, 1998; Vol. 3.
(32) Shu, S.; Li, Z.; Li, Y. Y. Triple-layer Fabry-Perot absorber with near-perfect absorption in visible and near-infrared regime. *Opt. Express* **2013**, *21*, 25307−25315.
(33) Lee, B.; Zhang, Z. Design and fabrication of planar multilayer structures with coherent thermal emission characteristics. *J. Appl. Phys.* **2006**, *100*, 063529.
(34) Cui, Y.; He, Y.; Jin, Y.; Ding, F.; Yang, L.; Ye, Y.; Zhong, S.; Lin, Y.; He, S. Plasmonic and metamaterial structures as electromagnetic absorbers. *Laser Photonics Rev.* **2014**, *8*, 495−520.
(35) Zhang, J.; Ou, J.-Y.; Papasimakis, N.; Chen, Y.; MacDonald, K. F.; Zheludev, N. I. Continuous metal plasmonic frequency selective surfaces. *Opt. Express* **2011**, *19*, 23279−23285.
(36) Tan, S. J.; Zhang, L.; Zhu, D.; Goh, X. M.; Wang, Y. M.; Kumar, K.; Qiu, C.-W.; Yang, J. K. Plasmonic color palettes for photorealistic printing with aluminum nanostructures. *Nano Lett.* **2014**, *14*, 4023−4029.
(37) Furchi, M.; Urich, A.; Pospischil, A.; Lilley, G.; Unterrainer, K.; Detz, H.; Klang, P.; Andrews, A. M.; Schrenk, W.; Strasser, G. Microcavity-integrated graphene photodetector. *Nano Lett.* **2012**, *12*, 2773−2777.
(38) Xia, F.; Mueller, T.; Lin, Y.-m.; Valdes-Garcia, A.; Avouris, P. Ultrafast graphene photodetector. *Nat. Nanotechnol.* **2009**, *4*, 839−843.

DOI: 10.1021/ph500410u
ACS Photonics 2015, 2, 183−188